# Hydrostatic Stress Effect on the Yield Behavior of Inconel 100

Phillip A. Allen[1] and Christopher D. Wilson[2]

[1]*Strength Analysis Group/ED22, NASA Marshall Space Flight Center*
*Marshall Space Flight Center, AL 35812, USA*
*256-544-1189 voice, 256-544-7234 fax*
*phillip.a.allen@nasa.gov*
[2]*Department of Mechanical Engineering, Tennessee Technological University*
*P.O. Box 5014, Cookeville, TN 38505-0001*
*931-372-3216 voice, 931-372-6340 fax*
*chriswilson@tntech.edu*

**ABSTRACT**

Classical metal plasticity theory assumes that hydrostatic stress has a negligible effect on the yield and postyield behavior of metals. Recent reexaminations of classical theory have revealed a significant effect of hydrostatic stress on the yield behavior of various geometries. Fatigue tests and nonlinear finite element analyses (FEA) of Inconel 100 (IN100) equal-arm bend specimens and new monotonic tests and nonlinear finite element analyses of IN100 smooth tension, smooth compression, and double-edge notch tension (DENT) test specimens have revealed the effect of internal hydrostatic tensile stresses on yielding. Nonlinear FEA using the von Mises (yielding is independent of hydrostatic stress) and the Drucker-Prager (yielding is linearly dependent on hydrostatic stress) yield functions were performed. A new FEA constitutive model was developed that incorporates a pressure-dependent yield function with combined multilinear kinematic and multilinear isotropic hardening using the ABAQUS user subroutine (UMAT) utility. In all monotonic tensile test cases, the von Mises constitutive model, overestimated the load for a given displacement or strain. Considering the failure displacements or strains for the DENT specimen, the Drucker-Prager FEM's predicted loads that were approximately 3% lower than the von Mises values. For the failure loads, the Drucker Prager FEM's predicted strains that were up to 35% greater than the von Mises values. Both the Drucker-Prager model and the von Mises model performed equally well in simulating the equal-arm bend fatigue test.

## INTRODUCTION

Since the 1940's, many have considered Bridgman's /1/ experiments on the effects of hydrostatic pressure on metals the definitive study. Bridgman's two observations about metal behavior were that hydrostatic stress has a negligible effect on yielding of metals and that metal is incompressible for plastic strain changes. These two observations have become the standard tenets for studies in metal plasticity. Because of the influence of Bridgman's work, plasticity textbooks from the earliest (e.g. Hill /2/) to the most modern (e.g. Lubliner /3/) infer that there is negligible hydrostatic stress effect on the yielding of metals. Even modern finite element programs such as ANSYS /4/ and ABAQUS /5/ direct the user to assume the same. Calculations are often made based on the assumption that the effect of hydrostatic stress is negligible. In certain circumstances though, the effects of hydrostatic stress can have a significant influence on material yield behavior.

The hydrostatic or mean stress is

$$\sigma_m = \frac{I_1}{3} = \frac{\sigma_1 + \sigma_2 + \sigma_3}{3}, \tag{1}$$

and the hydrostatic pressure, $p$ is $-\sigma_m$. The term $I_1$ is the first stress invariant and $\sigma_1$, $\sigma_2$, and $\sigma_3$ are the three principal stresses. It is well documented that large tensile hydrostatic stresses develop in sharply notched or cracked geometries /6-9/. Wilson /10,11/ and Allen /12,13/ have demonstrated that for these cases, a yield criterion that is dependent on hydrostatic stress, such as the Drucker-Prager yield criterion, produces results that better match monotonic test data. Therefore, it was postulated that a pressure-dependent yield function would also lead to more accurate prediction of specimen behavior in monotonic and low cycle fatigue (LCF) loadings of notched Inconel 100 (IN100) components.

The objective of this study was to examine the effect of hydrostatic stress on the yield behavior of IN100. The first research task was to conduct mechanical tests to determine accurate material properties for IN100 for use in nonlinear finite element analyses. The second part of the research was to compile load-displacement or load-microstrain test data from IN100 test geometries with varying amounts of hydrostatic tensile stress. The final research task was to model the behavior of the specimens using hydrostatic independent and hydrostatic dependent constitutive models in nonlinear finite element analyses and to compare the FEA results with the actual test data.

## PRESSURE-DEPENDENT PLASTICITY

Bridgman continued to study the effects of external hydrostatic pressure for many years, and, in 1952, he wrote a comprehensive summary of his work in his book *Studies in Large Plastic Flow and Fracture with Special Emphasis on the Effects of Hydrostatic Pressure* /14/. In this book, he reexamined his earlier results and made observations that many plasticity books failed to notice. On p. 64 of his book, Bridgman writes:

"By the time the last series of measurements was being made under the arsenal contract, however, skill in making the measurements had so increased, and probably also the homogeneity of the material of the specimens had also increased because of care in preparation, that it was possible to establish a definite effect of pressure on the strain hardening curve". /14/

For example, Bridgman's tests found that the flow stress for tempered pearlite at a strain of 2.75 increased from 1758 MPa (255 ksi) at atmospheric pressure to 2171 MPa (315 ksi) when pressurized to approximately 2482 MPa (360 ksi). Therefore, Bridgman clearly demonstrated in his later work a definite external hydrostatic pressure effect on yielding.

In the 1970's and early 1980's Spitzig, Richmond, and Sober /15,16,17,18/ also conducted experiments to study the effects of hydrostatic pressure on yield strength for four steels (4310, 4330, maraging steel, and HY80) and grade 1100 aluminum. They conducted compression and tension tests on smooth specimens in a Harwood hydrostatic-pressure unit at pressures up to 1100 MPa (160 ksi).

Spitzig, *et al.* found that hydrostatic pressure had a significant effect on the stress-strain response of the steels. For example, the compressive yield strength of the 4330 steel increased from 1520 to 1610 MPa (220 to 234 ksi) as pressure was increased to 1100 MPa (160 ksi), and for the aged maraging steel, the compressive yield strength increased from 1810 to 1890 MPa (263 to 274 ksi) as pressure was increased to 1100 MPa (160 ksi).

Spitzig *et al.* also found that the yield strength was a linear function of hydrostatic pressure as shown in Figure 1. Spitzig proposed that for metals the yielding process is described by the yield function

$$f(I_1, J_2) = \sqrt{3J_2} + aI_1 - d, \tag{2}$$

where $J_2$ is the second deviatoric stress invariant, $d$ is the modified yield strength in absence of mean stress and $a$ is a material constant related to the theoretical cohesive strength of the material, $\sigma_c$. Equation (2) is identical to the yield function originally proposed by Drucker and Prager /19/ to solve soil mechanics problems. As illustrated in Figure 1, the material constant $a$ is determined graphically as the slope of the graph of $\sigma_{eff}$ versus $I_1$ and can be written in terms of the tensile and compressive yield strengths as

$$a = \frac{\sigma_{ysc} - \sigma_{ys}}{\sigma_{ysc} + \sigma_{ys}}. \tag{3}$$

The value of $I_1$ for $\sigma_{eff} = 0$ is equal to the theoretical cohesive strength of the material, and the value of $I_1 = 0$ leads to $\sigma_{eff} = d$. Values of $a$ and $d$ reported by Spitzig, *et al.* /18/ and Chen /20/ are listed in Table 1.

Another interesting result that emerged from Spitzig's tests was a strong correlation between the coefficients $a$ and $d$. He found that the ratio of $a/d$ was nearly constant for most of the steels as listed in Table 1. Spitzig also suggested that the ratio $a/d$ is a property of the bulk iron lattice in a manner similar to the elastic constants Young's modulus, $E$, and Poisson's ratio, $\nu$.

Spitzig *et al.* also conducted pressurized compression and tension tests on two polymers—crystalline polyethylene and amorphous polycarbonate. These tests were performed to see if the plasticity theories developed for metals were compatible with other materials. They found that hydrostatic pressure had a significant effect on the stress-strain response of the polymers and that the effective stress was a linear function of hydrostatic pressure. In other words, Richmond established that the polymers' plastic response could be described by the same plasticity theories that he developed for metals. Therefore, the fact that soils,

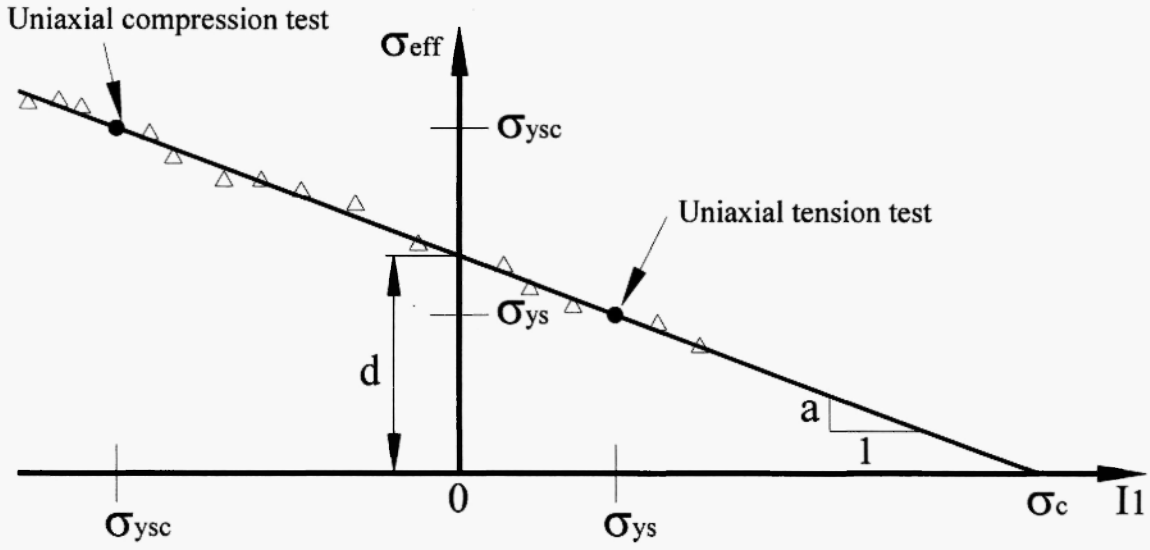


**Fig. 1:** Schematic of $\sigma_{eff}$ versus $I_1$ /15/.

**Table 1**

Summary of Experimental Results for Constants in Equation (2) /18,20/

| Material Name | *a* | *d*, MPa (ksi) | *a*/*d*, MPa-1 |
|---|---|---|---|
| HY80 Steel | 0.008 | 606 (88) | $13\times10^{-6}$ |
| Unaged Maraging Steel | 0.017 | 1005 (146) | $17\times10^{-6}$ |
| 4310 Steel | 0.025 | 1066 (154) | $23\times10^{-6}$ |
| 4330 Steel | 0.025 | 1480 (215) | $17\times10^{-6}$ |
| Aged Maraging Steel | 0.037 | 1833 (266) | $20\times10^{-6}$ |
| 1100 Aluminum | 0.0014 | 25 (3.6) | $56\times10^{-6}$ |
| Polyethylene | 0.022 | 13 (1.9) | $17\times10^{-4}$ |
| Polycarbonate | 0.011 | 36 (5.2) | $31\times10^{-5}$ |
| Clay | 0.118 | $6.7\times10^{-2}$ ($9.7\times10^{-3}$) | 1.76 |

metals, and polymers are all affected in a similar manner as described by the pressure terms in the Drucker-Prager yield function (Equation (2)) is a unifying concept.

The Drucker-Prager yield surface is a right-circular cone in principal stress space as shown in Figure 2.

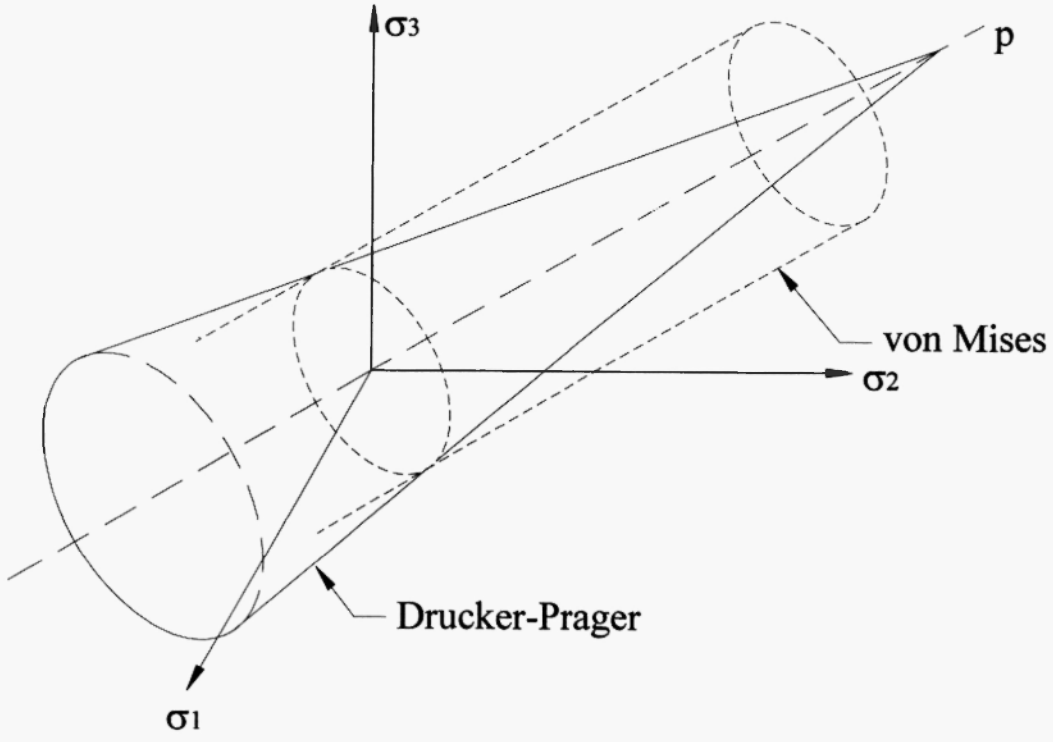


**Fig. 2:** Drucker-Prager and von Mises Yield Surfaces in Principal Stress Space.

The axis of the cone is the hydrostatic pressure axis, and the apex of the cone is located at a hydrostatic stress equal to the cohesive strength. The yield surface for an actual material probably does not come to a sharp apex as the linear Drucker-Prager model predicts. The sharp point of the cone could cause numerical difficulty in calculating derivatives for flow calculations, and, therefore, the finite element code ABAQUS provides hyperbolic and exponential Drucker-Prager constitutive models that round off the closed end of the cone /5/. For small amounts of hydrostatic stress, the cylinder of the von Mises yield criterion can approximate the cone. As the hydrostatic stress increases, the deviation from the cylinder can be considerable, and the Drucker-Prager yield surface is preferable. Because of its hydrostatic dependency, the Drucker-Prager yield criterion should result in more accurate modeling of geometries that have a high hydrostatic stress influence such as cracks and notches.

## RESEARCH PROGRAM

### Inconel 100 Testing

NASA MSFC and Pratt and Whitney provided a limited amount of IN100 in the form of two small ring forgings. These two rings were machined to obtain 8 smooth tensile and 24 smooth compression specimens. Because a limited amount of material was available for machining into test specimens, NASA /21/ and Pratt and Whitney /22/ test data was used for the double-edge notch tension (DENT) and equal-arm bend analyses, respectively. Also, no specific tests were performed to determine the elastic constants $E$ and $\nu$. Instead, $E$ was estimated from the smooth tensile test data, and a value for $\nu$ of 0.30 was obtained from the *Aerospace Structural Metals Handbook* /23/. The details of the IN100 tests are presented below.

**Smooth tensile tests.** Four 6.35 mm (0.25 in.) diameter tensile specimens were machined from each of the two rings. Gage displacement was measured using a MTS 634-31E-24 adjustable gage length extensometer, set to a 12.7 mm (0.5 in.) gage length. All smooth uniaxial tension tests were performed in accordance with ASTM E8 /24/. A summary of the tensile data is given in Table 2.

**Table 2**
Summary of IN100 Smooth Tensile Results

| Statistical Measure | Young's Modulus, GPa ($10^3$ ksi) | Upper Yield Strength, MPa (ksi) | 0.2% Offset Yield Strength, MPa (ksi) | Ultimate Tensile Strength MPa (ksi) | True Fracture Strain |
|---|---|---|---|---|---|
| Average | 220 (31.8) | 1184 (172) | 1150 (167) | 1618 (235) | 0.230 |
| Standard Deviation | 1.99 (0.32) | 10.42 (1.49) | 20.26 (2.96) | 5.72 (0.82) | 0.010 |

**Smooth compression tests.** The IN100 uniaxial compression tests were performed at NASA MSFC. Three smooth compression cylinders, 28.56mm (1.125 in.) long by 9.53mm (0.375 in.) diameter, from each ring were tested. Gage displacement was measured using a MTS 632.26E-21 extensometer with a 7.62 mm (0.3 in.) gage length. All smooth uniaxial compression tests were performed in accordance with ASTM E9 /25/. The test apparatus was qualified per E9 without using lubrication between the specimens and the compression platens, and therefore all of the specimens were tested without lubricated ends. All of the tests were interrupted at 0.025 to 0.030 true strain to prevent damage to the extensometer.

The deformed compression specimens showed evidence of side-slip buckling, which usually is a result of misalignment of the loading train or loose end tolerance on specimen dimensions /26/. Side-slip buckling tends to lower the true stress-true strain curve and may have contributed to some test data scatter. Table 3 gives a summary of the compression data.

**Table 3**

Summary of IN100 Smooth Compression Results

| Statistical Measure | Young's Modulus, GPa ($10^3$ ksi) | Upper Yield Strength, MPa (ksi) | 0.2% Offset Yield Strength, MPa (ksi) |
|---|---|---|---|
| Average | 225 (32.6) | 1185 (172) | 1153 (167) |
| Standard Deviation | 2.17 (0.29) | 2.86 (0.41) | 3.61 (0.52) |

A comparison of representative compression and tensile true stress-true strain curves is given in Figure 3. The compressive and tensile behaviors are very similar. Young's modulus is approximately 2.5% higher for the compression tests, but the upper and 0.2% offset yield strengths are approximately the same.

It was originally postulated that the Drucker-Prager material constant, $a$, could be calculated using Equation (3) by comparing uniaxial tension and compression results. For the IN100 tests, though, the compressive and tensile yield strengths were practically identical. This implies a Drucker-Prager constant of approximately zero. Several researchers /26,27,28/ have demonstrated that lubricating the ends of the test specimens results in a more uniaxial state of stress and can shift the load displacement record for a

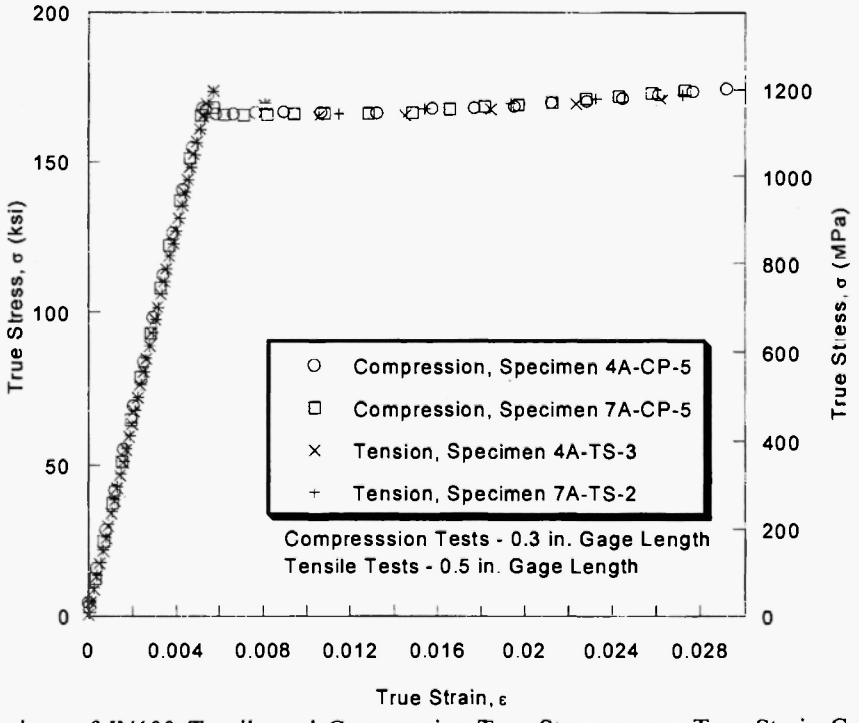


**Fig. 3:** Comparison of IN100 Tensile and Compressive True Stress versus True Strain Curves at Room Temperature.

compression test significantly upward. For example, Chait and Curll /27/ found that the Teflon lubricated compressive $\sigma - \varepsilon$ curve was from 2% to 15% higher than the unlubricated $\sigma - \varepsilon$ curve for 4340 steel. Equation (3) can be solved for $\sigma_{ysc}$ to give

$$\sigma_{ysc} = \frac{1+a}{1-a}\sigma_{ys}. \tag{4}$$

Substituting the value of $a$ for IN100 used in this research ($a$ = 0.022; See "Inconel 100 Material Property Inputs" for more detail on the selection of $a$.) into Equation (4) results in a $\sigma_{ysc}$ that is 4% higher that $\sigma_{ys}$. Therefore, if the IN100 compression cylinders were tested with lubrication on the ends, it is possible that the compressive load-displacement test record would shift upward. This shift would produce a differential between the compressive and tensile yield strengths and allow $a$ to be calculated using Equation (3).

**Double-edge notch tension tests.** Load-displacement test data was obtained from NASA /21/ for the double-edge notch tension specimen. An engineering drawing of the DENT specimen is given in Figure 4. Gage displacement was measured using a 12.7 mm (0.5 in.) gage length extensometer.

**Equal-arm bend three-cycle proof test.** Pratt and Whitney provided IN100 LCF data /22/ for a unique test specimen, the equal-arm bend specimen /29/. An engineering drawing of the equal-arm bend specimen is given in Figure 5. This specimen was designed to simulate the geometry and loading condition of a highly stressed area in the Space Shuttle main engine fuel turbopump housing.

A three-cycle proof test was performed on the equal-arm bend specimen. The specimen was pin loaded. A strain gage was bonded in the fillet, and the test was run in load control to achieve approximate strain levels.

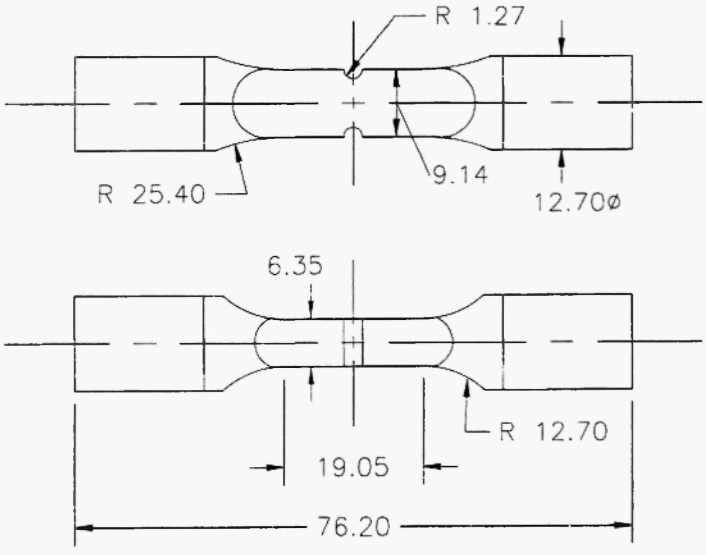


**Fig. 4:** Engineering Drawing of the DENT Specimen (Dimensions in mm).

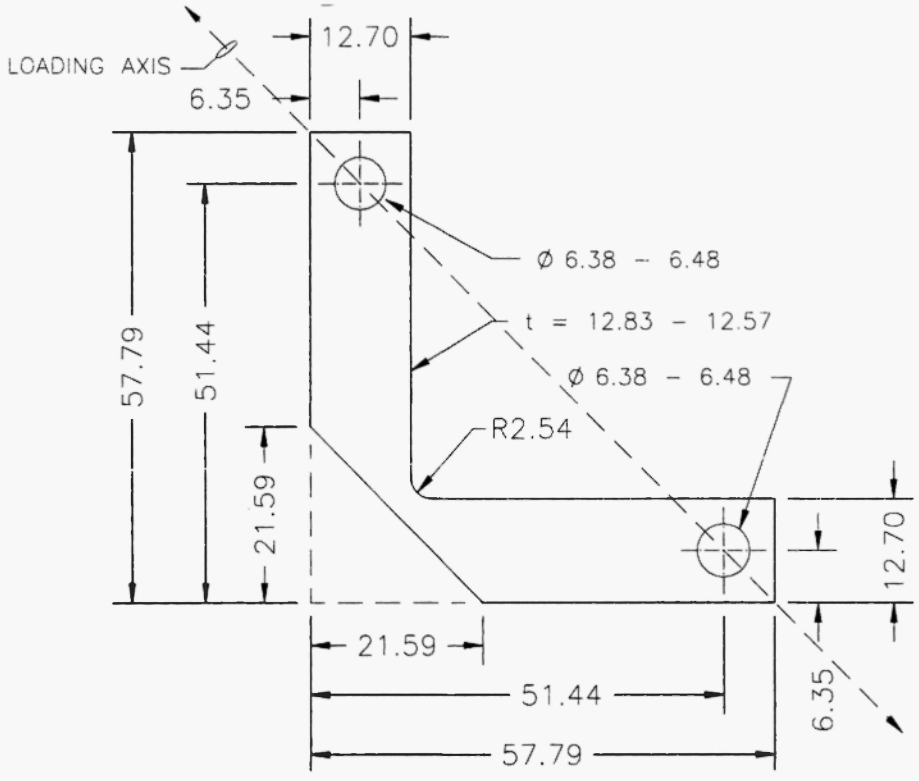


**Fig. 5:** Engineering Drawing of the Equal Arm Bend Specimen (Dimensions in mm).

On the first cycle, the specimen was loaded to 3% strain and then unloaded to 1.3% strain. The second cycle reloaded the specimen back to 3% strain and then unloaded to 1.3% strain. The third cycle was a repeat of the second cycle. The proof test was performed at 27° C (80° F) in air. Also, because the test was run in load control, there was some variance in the maximum and minimum strain values achieved for each cycle.

## Finite Element Modeling

Several finite element models were created for this research. The Sandia National Laboratory program FASTQ /30/ was used for preprocessing of meshes and boundary conditions for the smooth tensile and smooth compression geometries. The commercial finite element code Patran /31/ was used for the generation of the meshes and boundary conditions for the DENT and equal-arm bend geometries. ABAQUS /5/ was used for the finite element analyses and postprocessing the results. Full integration was used, and all of the FEM's were loaded in displacement control. Details of the finite element models are given by Allen /12,13/.

For all the geometries modeled, convergence studies were performed to determine the variation of effective stress, $\sigma_{eff}$, mean stress, $\sigma_m$, radial stress, $\sigma_{rr}$, (or the stress in the x-direction, $\sigma_{xx}$) and equivalent plastic strain, $\varepsilon^{pl}_{eq}$ across the neck or notch region at failure or maximum load for the three mesh densities

(coarse, medium, and fine). For all cases, the variation between the three mesh densities was very small until the outer surface of the neck or notch region was reached. The medium mesh models provided essentially the same results as the fine mesh models and computationally took approximately the same time as the coarse mesh models to run. Therefore, after completion of the convergence study, the medium mesh FEM's were chosen for use in all of the analyses.

**Smooth tensile bar specimen.** Axisymmetric FEM's of the IN100 smooth tensile specimen was created using 4-node axisymmetric elements (type CAX4 in ABAQUS). Only one-quarter of the tensile bar gage section was modeled by using two symmetry planes, and a uniform displacement was applied to the top nodes of the FEM. The neck diameter of the FEM was reduced approximately 0.127 mm (0.005 in.) to ensure necking in the gage region of the model. The coarse, medium, and fine meshes consisted of 158, 552, and 1070 elements, respectively.

**Smooth compression cylinder specimen.** Axisymmetric finite element models of a smooth compression cylinder were created to simulate the uniaxial compression tests. One quarter of the compression specimen geometry was modeled by using two symmetry planes and 4-node axisymmetric elements (type CAX4 in ABAQUS). A uniform downward displacement was applied to the top nodes of the FEM for the loading boundary condition. The coarse, medium, and fine compression cylinder meshes consisted of 150, 534, and 1008 elements, respectively.

**Double-edge notch tension specimen.** Three two-dimensional (2-D) DENT models were created by utilizing a coarse, medium, and fine mesh in the notch region. The 2-D models were created using 4-node plane stress elements (type CPS4 in ABAQUS). Only the gage section of the specimen was modeled by utilizing two planes of symmetry as illustrated in Figure 6. The coarse, medium and fine meshes had

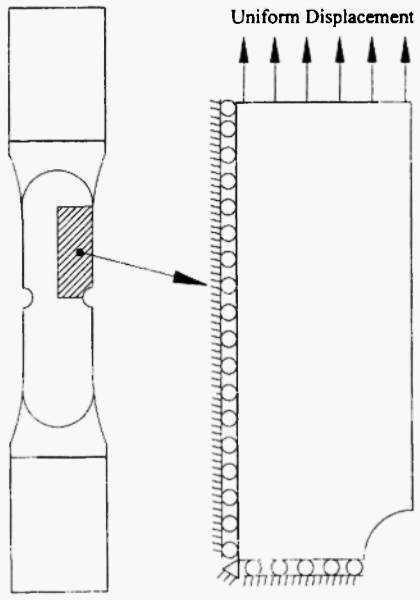


**Fig. 6:** Schematic of the 2-D DENT FEM Utilizing Two Symmetry Planes.

approximately 150, 300, and 630 elements in the notch region, respectively. An illustration of the 2-D DENT medium mesh FEM is given in Figure 7.

A 3-D DENT finite element model was created using 4740 8-node elements (type C3D8 in ABAQUS). Three symmetry planes were utilized in creating this FEM by dividing the specimen along the longitudinal axis, along the transverse axis, and through one-half of the thickness. The 3-D DENT finite element model's mesh corresponds to the medium mesh 2-D model extruded with 10 elements through the thickness.

**Equal-arm bend specimen.** The equal-arm bend finite element models were created using Q4 plane strain elements (type CPE4 in ABAQUS) and one symmetry plane. The symmetry plane and boundary conditions are illustrated in Figure 8. Plane strain elements were used because the thickness to width ratio in the fillet region was approximately 5 to 1. The load boundary condition was applied to the FEM by filling the hole for the loading-pin with elements and applying a displacement to the node in the center of the loading

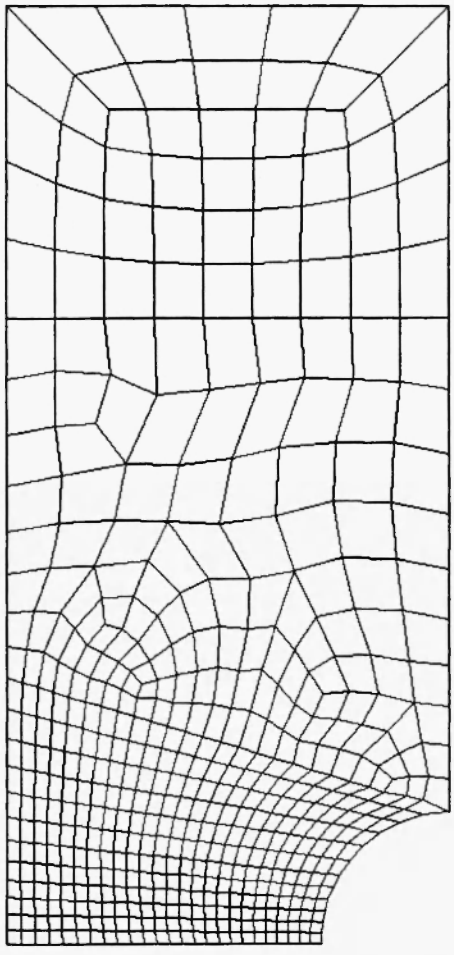

**Fig. 7:** Illustration of the 2-D DENT FEM.

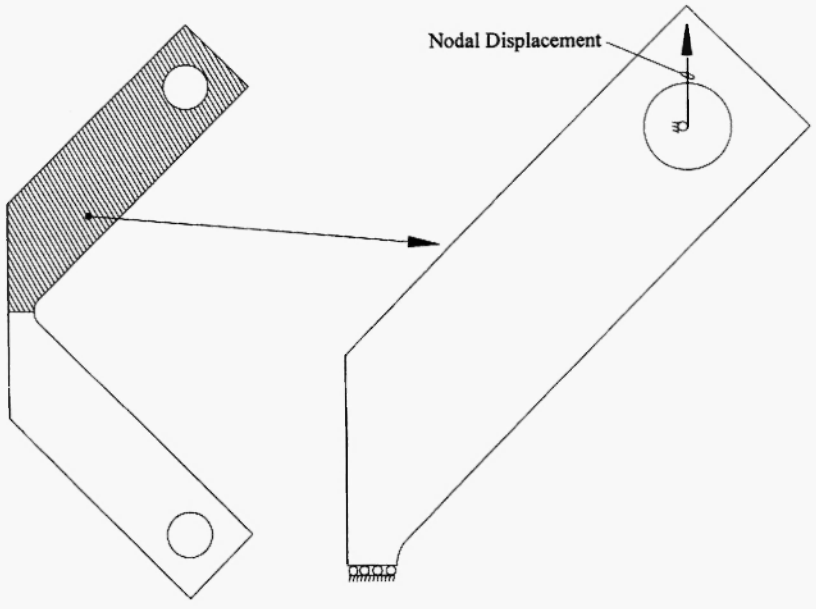


**Fig. 8:** Schematic of the Equal-Arm Bend FEM Utilizing One Symmetry Plane.

pin hole. The equal-arm bend coarse, medium, and fine meshes consisted of 1079, 1388, and 2469 elements, respectively. An illustration of the medium mesh FEM is given in Figure 9.

The modeling of the equal-arm bend three-cycle proof test offered an additional challenge. ABAQUS has built-in plastic flow models that allow bilinear kinematic hardening, multilinear isotropic hardening, or a nonlinear combination of kinematic and isotropic hardening when using the von Mises yield function. The Drucker-Prager yield function in ABAQUS, though, only allows isotropic hardening. Therefore, to realistically model the equal arm bend low cycle fatigue process using the Drucker-Prager yield function, it was necessary to develop a pressure-dependent constitutive model that incorporates a combination of multilinear kinematic and multilinear isotropic hardening. Assuming a linear combination of the two hardening types, a scalar parameter, $\beta$, can be defined which determines the amount of each type of hardening. It is a requirement that $0 < \beta < 1$. A value of $\beta = 1$ indicates only isotropic hardening, and a value of $\beta = 0$ indicates only kinematic hardening. The pressure-dependent constitutive model with combined hardening was implemented using the ABAQUS user subroutine (UMAT) function. The development of the UMAT and its implementation into ABAQUS are discussed in detail by Allen /13/.

## FEM Material Properties

Several material properties are required as input for the von Mises and Drucker-Prager constitutive models in ABAQUS. Both constitutive models require the material properties of Young's modulus, $E$, Poisson's ratio, $\nu$, and a table of true stress, $\sigma$, versus plastic strain, $\varepsilon^{pl}$. The Drucker-Prager model also

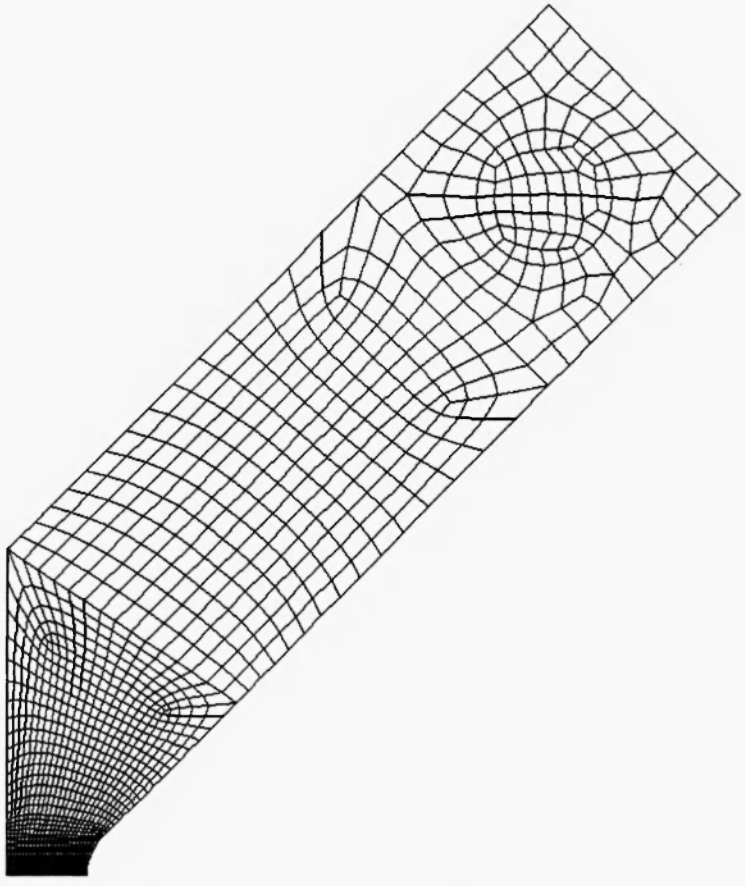

**Fig. 9:** Equal Arm Bend Finite Element Model Utilizing One Plane of Symmetry.

requires a value for the Drucker-Prager material constant, $a$. In addition, a value for the combined hardening parameter, $\beta$, is required for equal-arm bend low-cycle proof test model.

## RESULTS AND CONCLUSIONS

### Inconel 100 Material Property Inputs

The tensile IN100 material properties were obtained from the uniaxial tension tests and from the *Aerospace Structural Metals Handbook* /23/. The value for Poisson's ratio was 0.30, and the Drucker-Prager constant, $a$, was zero for von Mises plasticity. For Drucker-Prager plasticity, an iterative process using all of the FEM's was used to estimate a value for $a$ of 0.022. In other words, a value of $a$ was chosen to provide a reasonable match between the finite element simulations and the test data. A hardening parameter, $\beta$, of zero was chosen for all equal-arm bend FEM's to best match the first cycle hysteresis loop.

The values for Young's modulus used were 179 GPa ($26.0\times10^6$ psi) for the equal-arm bend FEM and 219 GPa ($31.8\times10^6$ psi) for the rest of the FEM's. The lower value of $E$ was used for the equal-arm bend specimen to match the test data in the linear range. The equal-arm test specimen was taken from a different lot of material than the material tested in this research. Also, Pratt and Whitney /29/ tensile test data for IN100 has widely scattered values for $E$ ranging from 172 to 241 GPa ($25.0\times10^6$ to $35.0\times10^6$ psi). Apparently the values for $E$ reported by Pratt and Whitney were estimated from tensile test data. In addition, some change in Young's modulus can be attributed to the variability in product form, such as castings versus forgings.

Considerable care was taken in developing the true stress versus plastic strain table. The test record of specimen 4A-TS-3 was chosen as representative of the tensile test data. Discrete data points from the actual test record were used to generate the table up to the point that the $\sigma$ - $\varepsilon^{pl}$ curve starts rolling over ($\varepsilon^{pl} \simeq 0.15$). The upper yield point was neglected in picking points for this portion of the table. After the $\sigma$ - $\varepsilon^{pl}$ curve rolls over, the test record no longer represents a uniaxial stress strain response due to necking of the test specimen. Therefore to generate the rest of the table, a straight line was fit between the last two points before the $\sigma$ - $\varepsilon^{pl}$ curve starts rolling over, and this line was projected out to a plastic strain of 1.0 to complete the data table.

**Smooth tensile bar results.** Load-gage displacement curves from the tensile bar FEM's are plotted along with a representative IN100 tensile test record in Figure 10. The von Mises curve slightly overestimates the

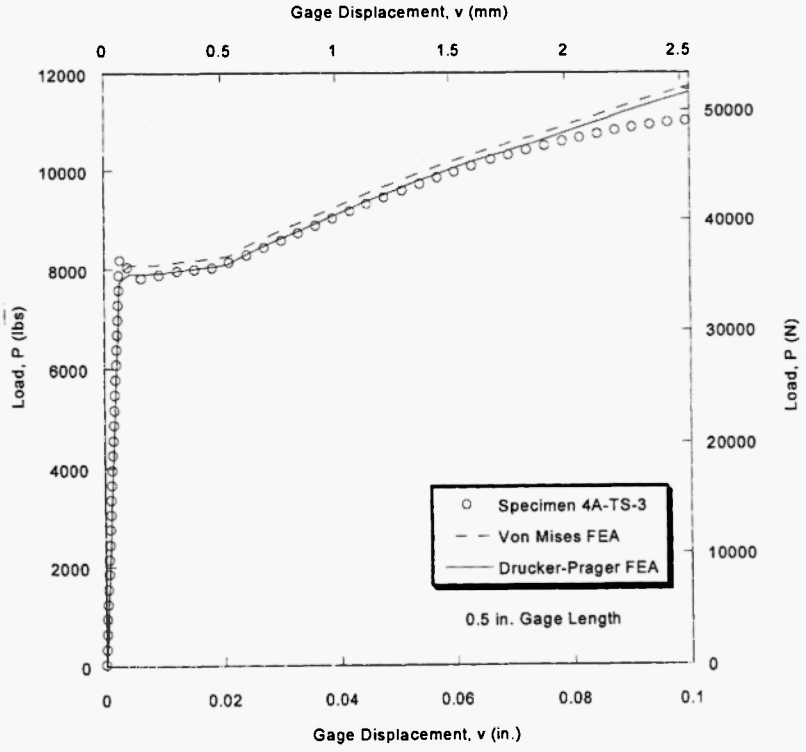


**Fig. 10:** Load-Gage Displacement Results for the Smooth Tensile Bar

load for a given value of displacement in the plastic region. The Drucker-Prager curve essentially matches the test data up to approximately 1.9 mm (0.075 in.) gage displacement. It is not surprising that both FEM's diverge from the test data after approximately 1.9mm gage displacement because the $\sigma - \varepsilon^{pl}$ table used by the FEM's also diverges from the test data at this point. In addition, both FEM's truncate the upper yield point due to the influence of the $\sigma - \varepsilon^{pl}$ table data.

**Smooth compression cylinder results.** Load-gage displacement curves from the smooth compression cylinder FEM's are plotted along with a representative IN100 compression test record in Figure 11. The von Mises solution slightly underestimates the load for a given displacement in the plastic region. Conversely, the Drucker-Prager solution slightly overpredicts the load for a given displacement in the plastic region. After approximately 0.23 mm (0.009 in.) gage displacement, both finite element solutions diverge from the test data.

**Double-edge notch tension results.** Load-displacement data for the medium mesh DENT 2-D and 3-D finite element models are plotted alongside NASA test data /21/ in Figure 12. Both the 2-D and 3-D von Mises FEM's overestimate the load for a given value of displacement in the postyield region. Considering the failure displacement, the Drucker-Prager FEM's predict loads that are about 3% lower than the von Mises values. For the failure load, the Drucker Prager FEM's predict strains that are about 35% greater than the von Mises values.

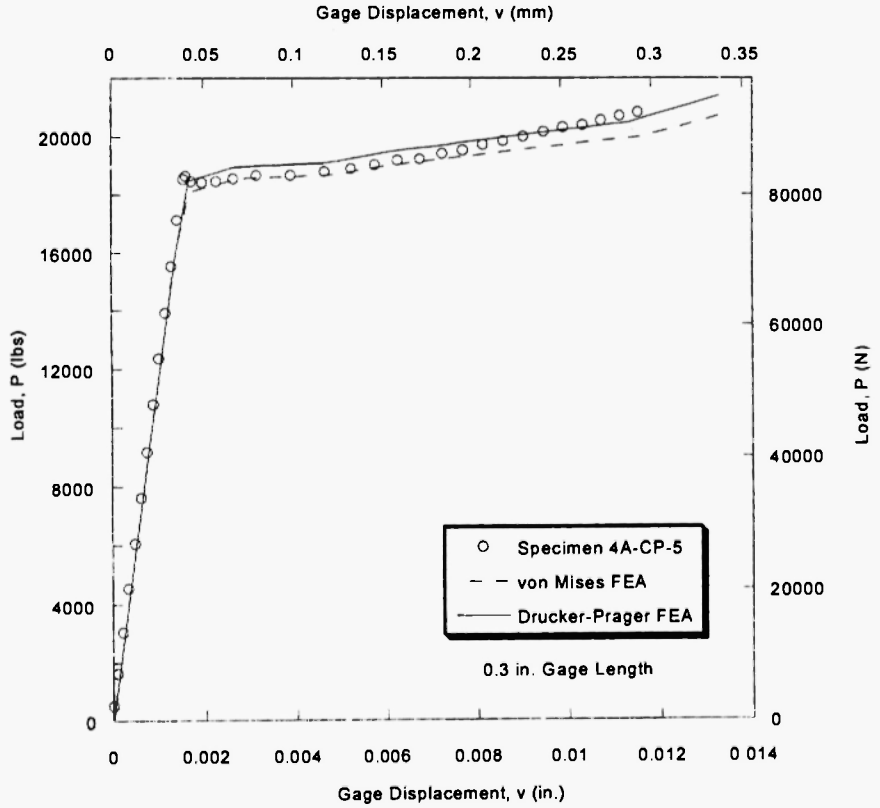


**Fig. 11:** Load-Gage Displacement Results for the Smooth Compression Cylinder.

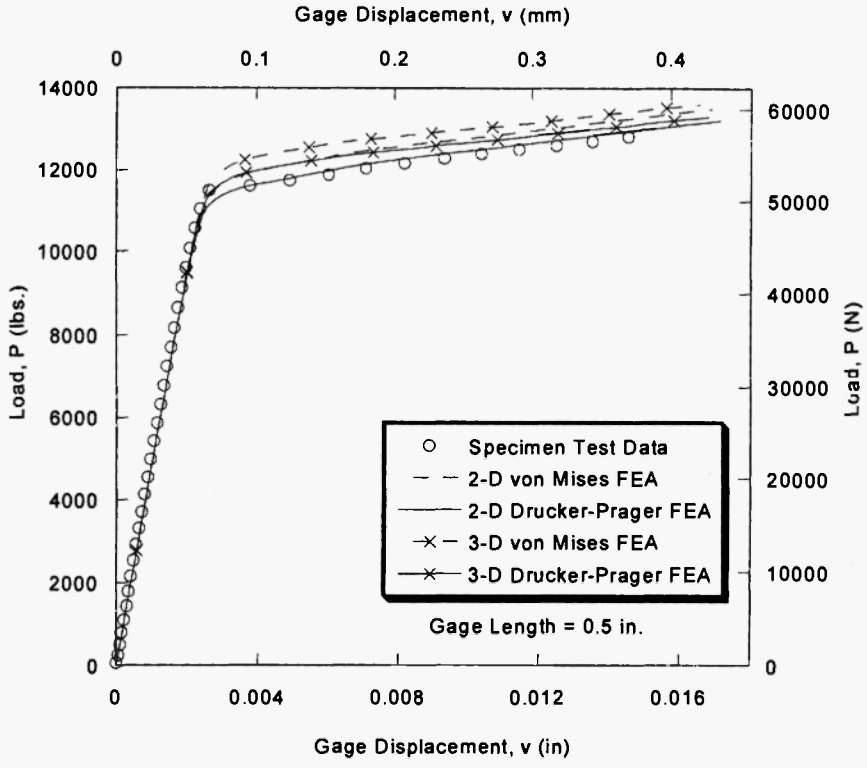


**Fig. 12:** 2-D and 3-D Load-Displacement Results for the DENT Specimen.

**Equal-arm bend results.** Load-microstrain test data for the first cycle is compared with the first cycle finite element analysis solutions in Figure 13. The von Mises and Drucker-Prager FEM's produce very similar results due to the combination of tensile and compressive bending stresses applied to the fillet region, which essentially negates the hydrostatic pressure influence in the fillet region. For the first cycle, both finite element solutions approximately match the test data until the negative loads are reached. Both models overestimate the first cycle minimum load by 34%. The second and third cycle equal arm bend results are given in Figures 14 and 15. The results for the second and third cycles are very similar. For both cycles, the FEM's underpredict the load for a given strain value on the loading cycles, but approximately match the maximum load. Also, both FEM's closely match the unloading data for cycles two and three.

## CONCLUSIONS

The following conclusions from this study of hydrostatic stress effects in yield behavior of IN100 are offered.

1. Using a yield function that is dependent on hydrostatic stress can significantly alter the predicted specimen response.

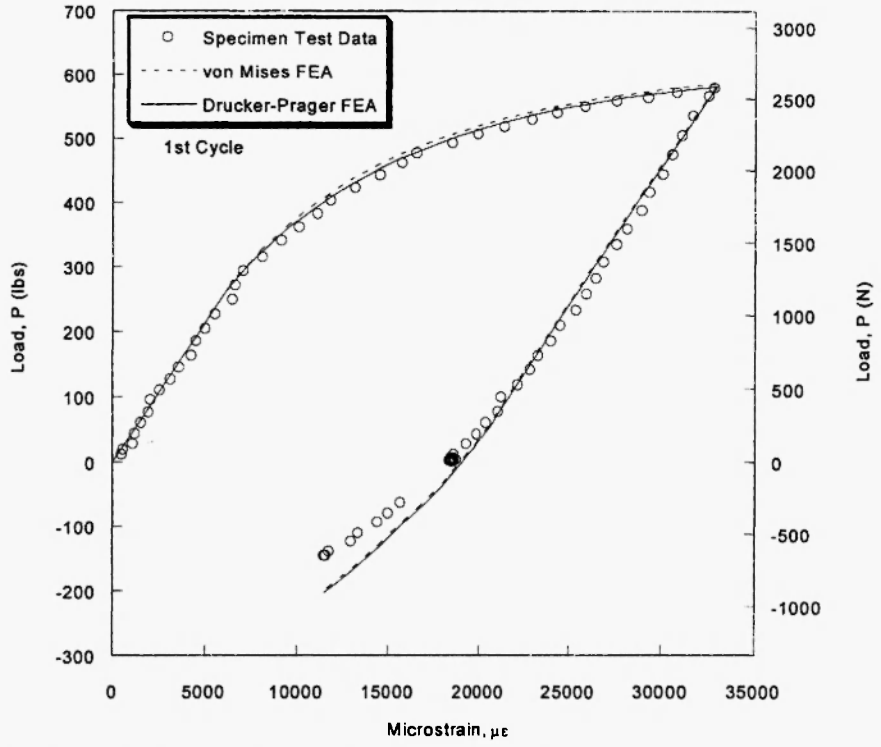


**Fig. 13:** First Cycle Load-Microstrain Results for the Equal-Arm Bend Specimen.

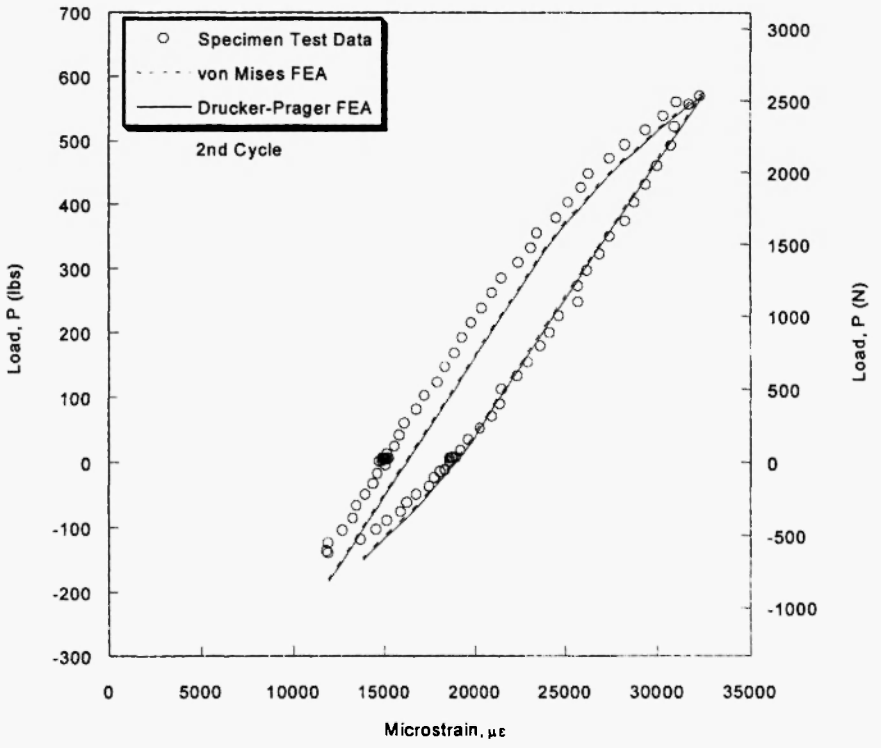


**Fig. 14:** Second Cycle Load-Microstrain Results for the Equal-Arm Bend Specimen.

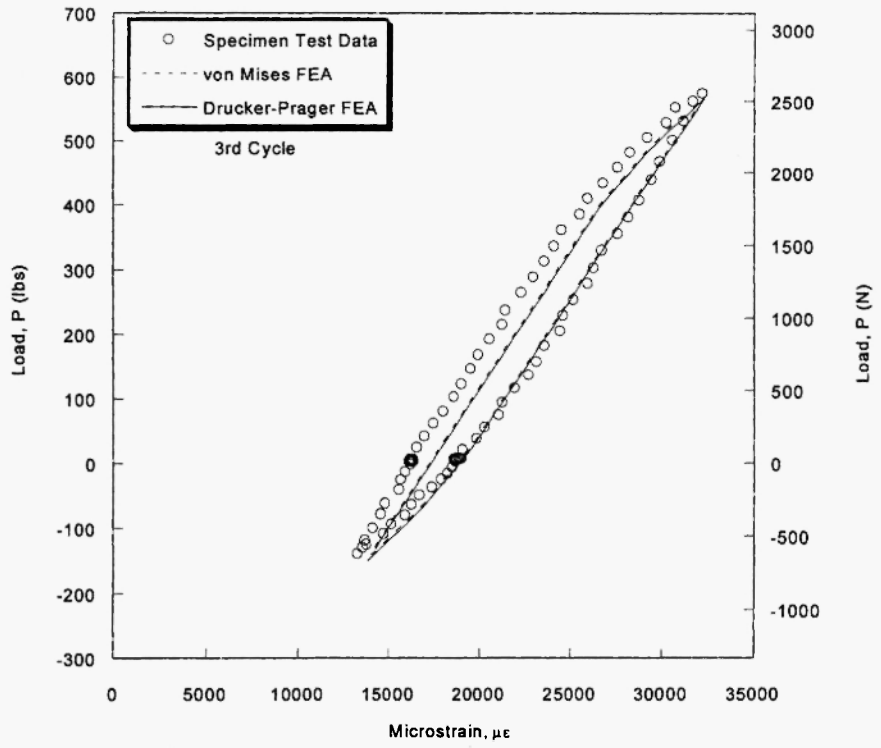


**Fig. 15:** Third Cycle Load-Microstrain Results for the Equal-Arm Bend Specimen.

2. For all tensile monotonic test cases, the von Mises constitutive model overestimated the load for a given displacement or strain.
3. For all tensile monotonic test cases, the Drucker-Prager constitutive model, which is a function of hydrostatic stress, produced results that better matched the test data. Considering the failure displacements or strains, the Drucker-Prager FEM's predicted loads that were approximately 3% lower than the von Mises values. For the failure loads, the Drucker-Prager FEM's predicted strains that were 20% to 35% greater than the von Mises values.
4. It is unclear whether the von-Mises or Drucker-Prager model is superior for simulating monotonic compressive behavior.
5. Both the Drucker-Prager and the von Mises model performed equally well in simulating the equal-arm bend three-cycle proof test.

## ACKNOWLEDGEMENTS

We would like to thank several people at Marshall Space Flight Center for their assistance, guidance, and advice. These people include Dr. Greg Swanson, Jeff Rayburn, Dr. Preston McGill, Doug Wells, Bill Malone, and Mike Watwood. We would also like to thank Bill Mitchell and Jerry Sheldon at Pratt and Whitney for providing Inconel 100 specimens and test data. Funding for this research was provided by the National Aeronautics and Space Administration (NASA) Graduate Student Researchers Program (GSRP).

## NOMENCLATURE

| Symbol | Description |
|---|---|
| $a$ | Slope of Effective Stress Versus the First Stress Invariant |
| $d$ | Modified Yield Strength |
| $f$ | Yield Function |
| $p$ | Hydrostatic Pressure |
| $E$ | Young's Modulus |
| $I_1$ | First Stress Invariant |
| $J_2$ | Second Deviatoric Stress Invariant |
| $P$ | Load |
| $\beta$ | Combined Hardening Parameter |
| $\varepsilon$ | True Strain |
| $\varepsilon^{pl}$ | Plastic Strain |
| $\varepsilon_{eq}^{pl}$ | Equivalent Plastic Strain |
| $\mu\varepsilon$ | Microstrain |
| $\nu$ | Poisson's Ratio |
| $\sigma$ | True Stress |
| $\sigma_c$ | Theoretical Cohesive Strength |
| $\sigma_{eff}$ | Effective Stress |
| $\sigma_m$ | Mean Stress |
| $\sigma_{ys}$ | Yield Strength |
| $\sigma_{ysc}$ | Compressive Yield Strength |
| DENT | Double-Edge Notch Tension |
| FEA | Finite Element Analysis |
| FEM | Finite Element Model |
| NASA | National Aeronautics and Space Administration |

## REFERENCES


1. Bridgman, P.W., 1947, "The effect of hydrostatic pressure on the fracture of brittle substances," *Journal of Applied Physics*, Vol. 18, p. 246.
2. Hill, R., 1950, "*The Mathematical Theory of Plasticity*," Clarendon Press, Oxford.
3. Lubliner, J., 1990, "*Plasticity Theory*," Macmillan, New York.
4. Kohnke, Peter, ed., 1994, "*ANSYS User's Manual for Revision 5.0*," *Volume IV: Theory.*
5. ABAQUS Theory Manual, Version 5.5, 1995, Hibbit, Karlsson, and Sorensen, Inc.
6. Neuber, Heinz, 1958, "Theory of Notch Stresses: Principles for Exact Calculation of Strength with Reference to Structural Form and Material," U.S. Atomic Energy Commission, ACE-tr-4547, Translated from publication of Springer-Verlag, Berlin, Gottingen, Heidelberg.
7. Hertzberg, Richard W., 1996, "*Deformation and Fracture Mechanics of Engineering Materials*," John Wiley & Sons, Inc., New York.
8. Rice, J.R., and D.M. Tracey, 1969, "On the ductile enlargement of voids in triaxial stress fields," *Journal of the Mechanics and Physics of Solids*, Volume 17, pp. 201-217.
9. Gurson, A.L., 1977, "Continuum theory of ductile rupture by void nucleation and growth: Part 1 – Yield criteria and flow rules for porous ductile media," *Journal of Engineering Materials and Technology*, Volume 99, pp 2-15.
10. Wilson, Christopher D., 1997, "Fracture Toughness Testing with Notched Round Bars," A Dissertation Presented for the Doctor of Philosophy Degree, The University of Tennessee, Knoxville.
11. Wilson, Christopher D., 2002, "A critical reexamination of classical metal plasticity," *The Journal of Applied Mechanics*, Volume 69, pp. 63-68.
12. Allen, Phillip A., 2000, "Hydrostatic Stress Effects in Metal Plasticity," A Thesis Presented for the Masters of Science Degree, Tennessee Technology University.
13. Allen, Phillip A., 2002, "Hydrostatic Stress Effects in Low Cycle Fatigue," A Dissertation Presented for the Doctor of Philosophy Degree, Tennessee Technology University.
14. Bridgman, P.W., 1952, "*Studies in Large Plastic Flow and Fracture with Special Emphasis on the Effects of Hydrostatic Pressure*," McGraw-Hill, New York.
15. Richmond, O., and W.A. Spitzig, 1980, "Pressure dependence and dilatancy of plastic flow," *International Union of Theoretical and Applied Mechanics Conference Proceedings*, pp. 377-386.
16. Spitzig, W.A., R.J. Sober, and O. Richmond, 1975, "Pressure dependence of yielding and associated volume expansion in tempered Martensite," *ACTA Metallurgica*, Volume 23, pp. 885-893.
17. Spitzig, W.A., R.J. Sober, and O. Richmond, 1976, "The effect of hydrostatic pressure on the deformation behavior of maraging and HY-80 steels and its implications for plasticity theory," *Metallurgical Transactions A*, Volume 7A, pp. 377-386.
18. Spitzig, W.A. and O. Richmond, 1984, "The effect of pressure on the flow stress of metals," *ACTA Metallurgica*, Vol. 32, No. 3, pp. 457-463.

19. Drucker, D.C., and W. Prager, 1952, "Soil mechanics and plastic analysis for limit design," *Quarterly of Applied Mathematics*, Volume 10, pp. 157-165.
20. Chen, W.F., and X.L. Liu, 1990, "*Limit Analysis in Soil Mechanics*," Elsevier, New York.
21. McGill, Preston, August 1999, DENT Test Data, ED33 Metallic Materials and Processes Group, NASA George C. Marshall Space Flight Center.
22. Pratt & Whitney, Nov. 16, 1999, Report Number MME 42030.
23. Manson, S.S., 1988, "*Aerospace Structural Metals Handbook*," Syracuse University Research Institute, Mechanical Properties Data Center, Mich.
24. American Society of Testing and Materials, 1998, E8 "Standard Test Methods for Tension Testing of Metallic Materials," 1998 Annual Book of ASTM Standards, Vol. 03.01, Philadelphia.
25. American Society of Testing and Materials, 1989, E9 "Standard Test Methods of Compression Testing of Metallic Materials at Room Temperature," 1989 Annual Book of ASTM Standards, Vol. 03.01, Philadelphia.
26. Kuhn, Howard A., 2000, "Uniaxial Compression Testing," ASM Handbook Vol. 8, Mechanical Testing and Evaluation.
27. Chait, R. and C.H. Curll, 1976, "Evaluating engineering alloys in compression," Recent Developments in Mechanical Testing, ASTM STP 608, American Society for Testing and Materials, pp. 3-19.
28. Hsü, T.C., 1969, "A study of the compression test for ductile materials," *Materials Research and Standards*, December.
29. Pratt and Whitney, 1991, "*Alternate Turbopump Development (ATD) Materials Manual*."
30. Blacker, T.D., 1988, "FASTQ Users Manual Version 1.2," Sandia Report SAND88-1326, UC-705, Sandia National Laboratories.
31. MSC Software Corporation, 2000, "Patran Users Manual", Version 9.0.